# Extreme mantle uplift and exhumation along a transpressive transform fault

Marcia Maia, Susanna Sichel, Anne Briais, Daniele Brunelli, Marco Ligi, Nicolas Ferreira, Thomas Campos, Berengere Mougel, Isa Brehme, Christophe C Hémond, et al.

**Nature Geoscience**
August 2016, Volume 9 Issue 8 Pages 619-+
http://dx.doi.org/10.1038/NGEO2759
http://archimer.ifremer.fr/doc/00345/45603/




# Extreme mantle uplift and exhumation along a transpressive transform fault

Maia Marcia [1, *], Sichel Susanna [2], Briais Anne [3], Brunelli Daniele [4, 5], Ligi Marco [5], Ferreira Nicolas [1], Campos Thomas [6], Mougel Berengere [1, 7], Brehme Isa [2], Hemond Christophe [1], Motoki Akihisa [8], Moura Denise [9], Scalabrin Carla [10], Pessanha Ivo [11], Alves Eliane [2], Ayres Arthur [2], Oliveira Pedro [2]

[1] Univ Bretagne Occidentale, CNRS, IUEM, Lab Domaines Ocean, Rue Dumont dUrville, F-29280 Plouzane, France.
[2] Univ Fed Fluminense, LAGEMAR, Ave Gal Milton Tavares Souza S-N, BR-24210340 Niteroi, RJ, Brazil.
[3] Univ Toulouse, GET, Ave Edouard Belin, F-31400 Toulouse, France.
[4] Univ Modena & Reggio Emilia, Dipartimento Sci Chim & Geol, Via Campi 103, I-41125 Modena, Italy.
[5] CNR, Geol Marina, ISMAR, Via Gobetti 101, I-40129 Bologna, Italy.
[6] Univ Fed Rio Grande do Norte, Dept Geol, Cidade Univ Lagoa Nova,CP 1639, BR-59072700 Natal, RN, Brazil.
[7] Inst Phys Globe Paris, 1 Rue Jussieu, F-75005 Paris, France.
[8] Univ Estado Rio de Janeiro, Ctr Tecnol & Ciencias, Inst Geociencias, Rua Sao Francisco, BR-20550013 Rio De Janeiro, Brazil.
[9] Univ Sao Paulo, Inst Astron Geofis & Ciencias Atmosfer, Rua Matao 1226,Cidade Univ, BR-05508090 Sao Paulo, Brazil.
[10] IFREMER, Lab Acoust, Technopole Iroise, F-29280 Plouzane, France.
[11] Brazilian Geol Survey, CPRM, Ave Pasteur 404, BR-22290255 Rio De Janeiro, Brazil.

* Corresponding author : Maia Marcia, email address : marcia.maia@univ-brest.fr

**Abstract :**

Mantle exhumation at slow-spreading ridges is favoured by extensional tectonics through low-angle detachment faults1, 2, 3, 4, and, along transforms, by transtension due to changes in ridge/transform geometry5, 6. Less common, exhumation by compressive stresses has been proposed for the large-offset transforms of the equatorial Atlantic7, 8. Here we show, using high-resolution bathymetry, seismic and gravity data, that the northern transform fault of the St Paul system has been controlled by compressive deformation since ~10 million years ago. The long-lived transpression resulted from ridge overlap due to the propagation of the northern Mid-Atlantic Ridge segment into the transform domain, which induced the migration and segmentation of the transform fault creating restraining stepovers. An anticlockwise change in plate motion at ~11 million years ago5 initially favoured extension in the left-stepping transform, triggering the formation of a transverse ridge, later uplifted through transpression, forming the St Peter and St Paul islets. Enhanced melt supply at the ridge axis due to the nearby Sierra Leone thermo chemical anomaly9 is responsible for the robust response of the northern Mid-Atlantic Ridge segment to the kinematic change. The long-lived process at the origin of the compressive stresses is directly linked to the nature of the underlying mantle and not to a change in the far-field stress regime.

When Darwin stopped in the St. Peter & St. Paul's islets in 1832, he recognised that the rocks exposed there were not volcanic and postulated that the mechanism for their formation was different from that building other oceanic islands[10]. The islets, formed by variably serpentinised and mylonitised peridotites[11,12], are currently uplifting at rates of 1.5 mm/yr[12]. Previous work suggested that the exposure of such large volume of ultramafic rocks resulted from an abnormally cold upper mantle[13-15] or cold lithosphere[16] in the Equatorial Atlantic and that the islets were either part of an extensional flexural ridge, as observed in other transform faults[6,13] or linked to compression[8]. Our data reveal that the islets are part of a major uplift of the lithospheric mantle due to a 10 Myr long period of transpression at the transform boundary[17]. Similar push-ups exist along continental strike-slip faults[18,19] but this is the first time one has been fully mapped in the oceanic lithosphere near a present-day spreading centre. Understanding the processes responsible for its formation will shed new light on the behaviour of large transform boundaries and their response to changes in both local and far-field stresses as well as on mechanisms leading to mantle exhumation at spreading centres.

Four transform faults and three intra-transform ridge segments, cumulating a 630 km offset, form the complex St. Paul transform system (Fig. 1 & Supplementary Fig. S1). Tectonic patterns and lithology reveal that the St. Peter & Paul's islets are part of a major, 200 km-long, 30 km-wide submarine shear zone that accommodates transpressive stresses along the northern transform fault of the St. Paul system[17] (Fig. 1). Most dredged samples are breccias of mylonitic peridotite and ultramylonites that underwent various degrees of serpentinisation and deformation (Supplementary Fig. S2). The morphology and the distribution of the deformation in the transform fault allow three tectonic domains in the shear zone to be defined: the Western Transfer Zone (WTZ), the Central Transpressive Zone (CTZ) and the Eastern Shear Zone (ESZ) (Fig. 2).

An important segmentation of the transform fault with associated push-up ridges resulting from dextral transpression characterizes the WTZ (Fig. 2a). Eastwards, a series of left-stepping restraining bends and offsets in the transform, associated with a large topography, form the distinct tectonic pattern of the CTZ. Thrust faults (Figs. 1, 2b & 3) mark the base of its south flank, overlapping the crust formed at the north intra-transform segment. These thrust faults, imaged by seismic reflection data (Fig. 3), are associated with the exposure of mylonitised peridotites and deformed sediments at this crustal contact. They form positive flower structures resulting from transpression at the restraining offsets along the shear zone (Fig. 2b). The area is seismically very active and, while most of the events have strike-slip focal mechanisms, a few compressive events[20] near the islets confirm the presence of thrust faults. The ~3500 m-high Atobá Ridge, located at the largest offset of the transform fault, is a major push-up ridge in the centre of the wider transpressive feature, marking the location of the most intense deformation[21]. The gravity-derived density structure over this portion of the shear zone

and the nature of the rocks sampled on both the islets and the flanks of the Atobá ridge (Fig. 4 and Supplementary Figs. S2 & S3) imply the presence of a core of uplifted, relatively unaltered high-density mantle beneath the islets and an anomalously thick low density layer on the ridge flanks, especially the southern one. We suggest that the thickening of the low-density layer derives from a local deepening of the serpentinisation front. Accordingly, the 500°C isotherm, that can be considered the limit of the serpentinisation process[22], lies at a depth of 25 km below the Atobá ridge (Fig. 4) i.e. deeper than the inferred maximum depths of the low-density layer, supporting the idea that the low-density material is related to hydration of mantle rocks. In the ESZ (Fig. 2c), the transform fault crosses a deep basin similar to the transform fault basins observed elsewhere in the St. Paul system (Fig. 1 and Supplementary Fig. S1). The basin morphology suggests the absence of significant transpression in this section of the shear zone. Close to the intra-transform segment, the transform becomes a double fault. This reveals that even in the more linear part of the transform domain the motion is not purely strike-slip.

The oblique segments and the offsets disrupting the main trend of the western transform boundary developed after several episodes of southward propagation of the northeastern segment of the Mid-Atlantic Ridge (MAR) in the last 10 Myr, as revealed by the lengthening of its abyssal hills. The absence of asymmetric faulting at this large-offset ridge-transform intersection implies that the robust segment receives enough melt supply to counteract the cold-edge effect of the transform fault[23] (Figs. 1 & 2a). The short northern intra-transform segment, although comparatively less robust, did not retreat to accommodate the propagation of the MAR segment, leading to an overlap of both spreading segments. The morphology of the intra-transform segment, with sub-

parallel abyssal hills mapped on both flanks, and the basalt samples recovered on and off axis are consistent with spreading dominated by volcanic processes for at least the last 10 Myr. However, contrary to the MAR, this small segment did not increase in length, reflecting the difference in melt supply between the segments.

The change in the tectonics of the northern boundary of the St. Paul system started ~11 Ma, when a 5° counterclockwise change in the spreading direction between the South America and Nubia plates occurred, inducing extension at large-offset left-stepping transforms in the Central and Equatorial Atlantic[5,24]. The origin of the St. Paul transpressive shear zone relates to the way the spreading geometry locally adjusted to this plate motion change. We construct an evolutionary scenario describing the responses of the transform to a sequence of far and local stress changes (Fig. 5). The 11 Ma counterclockwise rotation locally resulted in the transtensional formation of a flexural transverse ridge along the northern border of the transform fault. This same event resulted in the synchronous growth of the Vema transverse ridge at 11°N[5]. Shortly after, the spreading ridge segments started to adjust to the new spreading geometry, with the lengthening of the MAR segment, while the intra-transform segment to the East remained roughly stable. As the MAR segment kept propagating south, the western part of the transform started to segment and this non-uniform adjustment resulted in the formation of restraining bends and offsets, inducing localized transpression on the western portion of the flexural transverse ridge. The resulting structure is bounded by low-angle thrusting along the external faults of the system (Fig. 2). The four lengthening events, marked by the steps in the transform boundary, correspond to progressively slower propagation rates, as the ridge geometry adjusted to the local stresses (Fig. 5). The oldest and largest offset corresponds to a fast

displacement of the western transform segment from its main trend. This event created the first compressive stresses at the transverse ridge. As the transform fault adjusted southwards during the second event, the increase in the fault segment offset induced higher stresses that begun to form the sigmoidal push-up Atobá ridge. The following episode, of smaller amplitude, formed a smaller restraining bend, continuing to sustain the uplift of the Atobá ridge and forming the southern part of the CTZ. The most recent evolution also displays southward deviations of the shear zone resulting in transpressive deformation in the WTZ. The morphology, focal mechanisms, and evidence for uplift in the Atobá Ridge show that transpression is still active in the western part of the shear zone. Such an active deformation implies that the plate boundary did not reach a steady-state geometry and that the changes in the spreading geometry are still being accommodated, although at relatively lower present-day rates. Despite their similar offset, the Vema and the northern St. Paul transform show a different sequence of adjustments both starting with the same kinematic change. The Vema transform reacted with a single short transtensive adjustment while St. Paul records a multiple set of events over a larger time-span. A plausible cause of this different behaviour is the influence of the Sierra Leone hotspot, which may have enhanced the magma supply of the MAR segment just north of St Paul transform[9]. Lengthening of ridge segments due to increased magma supply is well documented along the MAR[25] and may be an important mechanism here. Geochemical data[9,14,26] show the existence of a mantle composition boundary within the St. Paul system, with an enriched mantle beneath the MAR segment north of the system extending to the northern intra-transform segment. The volcanic morphology of these segments possibly reflects the nature of the mantle, which favours enhanced melting.

Continental shear zones where restraining step-overs result in transpressive flower-like structures and push-up ridges, exposing mylonites and ultra-mylonites at the surface are well documented[18,19]. The observed structural and petrologic patterns at the St Paul northern transform boundary are similar, with multi-segmented and sub-parallel faults away from the step-ups and oblique faults close to them. Associated thrust faults uplift large reliefs and expose deep rocks distributed along bands parallel to the main strike-slip fault zone, forming positive flower structures. At the centre of these features, the higher topography is associated with a push-up block, oblique faults and intense deformation[18, 21]. The MAR half-spreading rate (16 mm/yr)[27] yields convergence rates of 32 mm/yr at the step-overs and transpressive segments of the fault. This amount of shortening is sufficient to uplift a 100 km-long block by more than 3500 m, with present-day uplift rates of 1.5 mm/yr[12], comparable to those estimated for structures observed along continental strike-slip faults[18,19].

The evolution of the northern St. Paul plate boundary, where the southward migration of both the MAR segment and the transform fault is progressively accommodated through bends, offsets and oblique structures over a wide shear zone, lead to a particular situation in the mid-ocean ridge system, with long-lived regional-scale transpression along the transform. Whereas most exposed mantle rocks near mid-ocean ridges result from extensional tectonics along detachment faults, our study reveals that the peridotites and mylonites of the St. Peter & Paul's islets result from a major uplift of the oceanic lithosphere along a transpressive shear zone due to local stresses which have been active during a time much longer than usually necessary for a plate boundary to adjust to a kinematic change. This may also be the case along other major transform faults, although probably at a smaller scale. Here we show that even

large-offset transforms, materializing large contrasts in lithosphere thickness, may deform due to the local stresses induced by the increase in melt supply at the spreading ridge. Mantle composition and temperature may therefore trigger the local response of the lithosphere. To understand deformation at large transforms, mantle processes must not be neglected.

References

1. Dick, H. J. B., Lin, J. & Schouten, H. An ultra slow spreading class of ocean ridge. *Nature* **426,** 405–412 (2003).

2. Sauter, D. *et al.* Continuous exhumation of mantle-derived rocks at the Southwest Indian Ridge for 11 million years. *Nature Geoscience* **6,** 314–320 (2013)

3. Escartín, J. *et al.* Central role of detachment faults in accretion of slow-spreading oceanic lithosphere. *Nature* **455,** 790–794 (2008).

4. Smith, D. K., Escartin, J., Schouten, H. & Cann, J. R. Fault rotation and core complex formation: significant processes in seafloor formation at slow-spreading midocean ridges (Mid-Atlantic Ridge, 13–15°N). *Geochem. Geophys. Geosyst.* **9,** Q03003, doi:10.1029/2007GC001699 (2008).

5. Bonatti, E. *et al*. Flexural uplift of a lithospheric slab near the Vema transform (Central Atlantic): Timing and mechanisms. *Earth Planet. Sci. Lett.* **240,** 642–655 (2005).

6. Tucholke, B. E. & Schouten, H. Kane Fracture Zone. *Mar. Geophys. Res.* **10,** 1-39 (1988)

7. Bonatti, E. *et al*. Transform migration and vertical tectonics at the Romanche fracture zone, Equatorial Atlantic. *J. Geophys. Res*. **99,** 21779 -21802 (1994).

8. Palmiotto, C. *et al*. Nonvolcanic tectonic islands in ancient and modern oceans, *Geochem. Geophys. Geosyst*. **14,** 4698–4717 (2013).

9. Schilling, J.-G., Hanan, B.B., McCully, B., Kingsley, D. & Fontignie, D. Influence of the Sierra Leone mantle plume on the equatorial Mid-Atlantic Ridge: A Nd-Sr-Pb isotopic study. *J. Geophys. Res*. **99,** 12,005-12,028 (1994).

10. Darwin, C. Geological Observations on the Volcanic Islands and Parts of South America Visited During the Voyage of H.M.S. 'Beagle', 3rd ed. (Smith, Elder, London, 1891).

11. Melson, W.G., Jarosewich, E., Bowen, V.T., Thompson, G. St. Peter and St. Paul Rocks: a high-temperature, mantle-derived intrusion. *Science* **155,** 1532–1535 (1967).

12. Campos, T. F. C., Bezerra, F. H. R., Srivastava, N. K., Vieira, M. M. and Vita-Finzi, C. Holocene tectonic uplift of the St Peter and St Paul Rocks (Equatorial Atlantic) consistent with emplacement by extrusion. *Marine Geology* **271,** 177-186 (2010).

13. Hekinian, R. *et al.* Submersible observations of Equatorial Atlantic mantle: the St Paul Fracture Zone region. *Mar. Geophys. Res.* **21,** 529–560 (2000).

14. Schilling, J.G. *et al*. Thermal structure of the mantle beneath the equatorial Mid-Atlantic Ridge: inference from the spatial variation of dredged basalt glass compositions. *J. Geophys. Res.* **100,** 10057–10076 (1995).

15. Bonatti, E. Anomalous opening of the equatorial Atlantic due to an equatorial mantle thermal minimum. *Earth Planet. Sci. Lett.* **143,** 147-160 (1996).

16. Brunelli, D. & Seyler, M. Asthenospheric percolation of alkaline melts beneath the St. Paul region (Central Atlantic Ocean). *Earth Planet. Sci. Lett.* **289,** 393–405 (2010).

17. Maia, M. *et al.* Complex ridge-transform evolution and mantle exhumation at the St. Paul fracture zone system, Equatorial Atlantic. Preliminary results from the COLMEIA cruise. Abstract OS42A-01 presented at 2013 Fall Meeting, AGU, San Francisco, Calif., 9-13 Dec (2013).

18. Mann, P. Global catalogue, classification and tectonic origins of restraining and releasing bends on active and ancient strike-slip fault systems. In *Tectonics of Strike-Slip Restraining and Releasing Bends* **290,** 239–253 (Geological Society Special Publications, London, 2007)

19. Dair, L. & Cooke, M. L. San Andreas fault geometry through the San Gorgonio Pass, California. *Geology* **37,** 119-122 (2009).

20. Wolfe, C.J., Bergman, E.A. & Solomon, S.C. Oceanic transform earthquakes with unusual mechanism or locations: relation to fault geometry and state of stress in the adjacent lithosphere. *J. Geophys. Res.* **98,** 16187–16211 (1993).

21. McClay, K. & Bonora, M. Analog models of restraining stepovers in strike-slip fault systems. *AAPG Bulletin* **85,** 233-260 (2001).

22. Ulmer, P. & Trommsdorff , V. Serpentine stability to mantle depths and subduction-related magmatism. *Science* **268,** 858-861 (1995).

23. Ligi, M., Bonatti, E., Cipriani, A. & Ottolini, L. Water-rich basalts at mid-ocean ridge cold spots. *Nature* **434,** 66-69 (2004).

24. Ligi, M., Bonatti, E., Gasperini, L. & Poliakov, A. N. B. Oceanic broad multifault transform plate boundaries. *Geology* **30,** 11–14 (2002).

25. Gente, P. *et al.* Characteristics and evolution of the segmentation of the Mid-Atlantic ridge between 20°N and 24°N during the last 10 million years. *Earth Planet. Sci. Lett*. **129,** 55-71 (1995).

26. Le Voyer, M., Cottrell, E., Kelley, K. A., Brounce, M. & Hauri, E. H. The effect of primary versus secondary processes on the volatile content of MORB glasses: An example from the equatorial Mid-Atlantic Ridge (5°N–3°S), *J. Geophys. Res. Solid Earth* **120,** 125-144 (2015).

27. DeMets, C., Gordon, R. G. & Argus, D. F. Geologically current plate motions, *Geophys. J. Int*. **181,** 1–80 (2010).

## Acknowledgements

The COLMEIA marine expedition was funded by the French Ministry of Research through the grant to the Flotte Océanographique Française. Additional supporting grants came from CNRS-INSU program “Campagnes à la mer”, Labex MER and Région Bretagne, France, and from Universidade Federal Fluminense and CPRM, Brazil. M.L. acknowledges supporting grant PRIN 20125JKANY_002. We thank SECIRM, Brazilian Navy, for their help and support to this project. We are grateful to Captain G. Ferrand and his crew from research vessel L’Atalante and to the technical staff of GENAVIR for their help on acquiring the data presented here.

## Author contributions

M.M. and S.S. conceived the COLMEIA project. M.M. led the COLMEIA cruise. M.M, A.B. and D.B. acquired, processed and interpreted the different data sets and wrote the paper. M.L. provided complementary bathymetry data, processed and interpreted the different data sets and wrote the paper. N.F. interpreted the bathymetry data. E.A., A.A. and P.O. interpreted the seismic data for sediment thickness. D.M. built the crustal age model and acquired the data during the COLMEIA cruise. T.C., B.M., I.B., C.H., A.M., C.S. and I.P. acquired the data during the COLMEIA cruise.

## Additional information

Supplementary information is available in the online version of the paper. Reprints and permissions information are available online at www.nature.com/reprints. Correspondence and requests for materials should be addressed to M.M., Laboratoire Domaines Océaniques, CNRS-Université de Bretagne Occidentale, IUEM, Rue Dumont d'Urville, 29280 Plouzané, France, marcia.maia@univ-brest.fr.

Competing financial interests

The authors declare no competing financial interests.

Figure captions

Figure 1. 1a. Location of the St Paul shear zone and other notable features of the Equatorial Atlantic. The Sierra Leone hotspot[9] location is shown by the red star. 1b. Multibeam bathymetry of the St. Paul shear zone. A black star shows the location of the St. Peter & St. Paul's islets. The thick black lines represent the present-day active transform faults, with the arrows showing the direction of plate motions. The black lines with the ticks represent the thrust faults. The white lines show the present-day spreading axes. The labelled rectangles show the areas detailed in Figure 2.

Figure 2. Shaded bathymetry of three different portions of the northern St. Paul shear zone. 2a. West Transfer Zone (WTZ) displaying a multi-segmented transform fault sub-parallel to the current spreading direction and three en-echelon push-up ridges. 2b. Central Transpressive Zone (CTZ) displaying step-overs of the transform fault on either side of the St Peter and Paul's islets. The Atobá Ridge is located at the central step. The

313 base of the south flank of the CTZ displays a series of thrust faults. 2c. Eastern Shear
314 Zone (ESZ) where the transform fault crosses a deep basin. Fault captions as in Figure 1.
315
316 Figure 3. Fully migrated reflection seismic line crossing the St. Paul shear zone (a)
317 (location shown in the inset) and interpreted cartoon (b) showing the thrust faults at
318 depth associated with the mylonite exposures and the positive flower structure. The
319 sediment cover also shows intense deformation. The processing techniques are
320 described in the Methods section.
321
322 Figure 4. Thickness map of a 2800 kg/m$^3$ density layer, that can correspond to crust
323 and/or to altered mantle, derived from the gravity data and superimposed on a shaded
324 high-resolution bathymetry. The density distribution is consistent with the rocks
325 sampled in the islets and on the submarine flanks of the CTZ (Supplementary Figure S2).
326 The black lines show the depth of the 500 °C isotherm contoured at a 1 km step. The
327 model parameters and method of calculation are described in the Methods section. The
328 black star shows the St. Peter & Paul's islets. Fault captions as in Figure 1.
329
330 Figure 5. Sketch of the evolution of the St. Paul shear zone from a configuration prior to
331 the change in plate motion at ~11 Ma on the top to the present boundary geometry, on
332 the bottom. Blue areas mark extensional features, red are compressive and gray shows
333 the inactive parts of the ridge. The large arrows show the spreading directions and the
334 thin black vertical arrow show the propagation of the northern MAR segment. The thin
335 oblique arrows show the direction of the local stresses.
336
337 Methods

Gravity modelling.

The gravity data obtained during the cruise[28] were processed in the conventional way (Eötvos, drift and latitude corrections) to compute the free-air anomalies before being merged into a grid, together with satellite-derived free-air anomaly data[29,30] to obtain the free-air anomaly used in this study. The density model consists of three layers of constant density: the sediment cover, the crust or altered mantle (or their density proxy) and the normal mantle, respectively with densities of 2400, 2800 and 3300 kg/m$^3$ and 1030 kg/m$^3$ for the water. Modelled densities do not attempt to reproduce the complex reality inferred from the petrology, but consider densities that may be close to altered and serpentinised peridotites, mylonites and crustal rocks. To construct a sediment thickness grid, we used the values derived from the interpretation of the seismic lines obtained during the cruise as well as available data from older cruises and extrapolated them to the neighbouring areas. The sedimentary infill reaches 300 to 500 m in the nearby basins, but most of the area presents only relatively thin sediment cover (less than 100 m). As the seismic lines are spaced further apart than the echosounder sampling, the resolution of the sediment grid is not as good as the bathymetry, so for the model, we interpolated the high-resolution bathymetry[28] onto a 1 km step grid, compatible with the sediment thickness grid, after projecting all data from geographic degrees to UTM kilometres. From the bathymetry and the sediment thickness, we calculated the basement topography. To calculate the Mantle Bouguer anomaly, we assumed a constant, 6 km-thick "crust" (or its proxy, a 2800 kg/m$^3$ density layer), using the basement as the top of the layer. The gravity effect of this model was computed in the Fourier domain using the multi-layer method, developed to account for both rapidly varying topography and shallow water depths[30] and subtracted from the free-air

anomaly grid yielding the Mantle Bouguer anomaly. Before inverting for the layer thickness variations from the assumed 6 km constant "crust", we removed the effect of the cooling of the lithosphere. Several thermal models were tested: a simple age model[31,32] and passive flow models[33,34] using different values for the thermal conductivity. As differences were only minor between the model results and expressed mostly as a broad regional trend, we chose to keep the age model. Moreover, the passive flow models tend to overemphasize the cold-edge effect, which our bathymetry data suggest is not so marked here, despite the large offset. The 2800 kg/m$^3$ layer thickness displayed in Figure 4 is obtained by adding the computed thickness variations to the 6 km thick "crust".

Seismic processing

The seismic lines were acquired with a 24 channels streamer using two air guns with 105 and 85 cubic inches[28]. All lines were processed using software Sispeed v5.5 developed by IFREMER. Common mid-point gathers were stacked and migrated using a simple velocity model with a sound velocity of 1500 m/s assigned for both water and sediments. After processing, interpretation was performed using Kingdom 8.5 software. The quality of the seismic lines in this rough topography area was checked by comparison between the sea bottom reflector derived from the seismic profiles and the topography derived from the high-resolution multibeam bathymetry. Only in a few areas, where the seismic lines closely parallel high scarps, significant differences due to lateral echoes were found. A few seismic lines crossing the CTZ were migrated with a more complex model for the velocity of the sound in the sediments and the basement, accounting for the increase in the sound velocity with depth, in order to better identify the reflectors in the basement. The model consists of a sediment layer with a velocity of

1750 m/s followed by a 300 m thick layer with a velocity of 2000 m/s and then a series of 500 m-thick layers with a velocity increase of 500 m/s each. The last horizon, at a depth of 5800 m from the top of the oceanic crust, seismically separates the crust from the mantle with a velocity 7500 to 8000 m/s. The line shown in Figure 3 was processed with this full migration model.

## Crustal age modelling

Since the proximity of the magnetic equator hinders the identification of magnetic anomalies, we analysed the evolution of this part of the St. Paul system through a kinematic reconstruction using the most recently published poles of rotation[35]. Theoretical crustal ages were calculated using the present day geometry of the mid-oceanic ridge and these poles.

## Data availability

Gravity and seismic data were acquired during the COLMEIA cruise[28]. The multibeam bathymetry used in this work came mainly from the COLMEIA cruise[28], completed with data from PRIMAR96[36] and S7 (R/V Strakhov)[37] cruises. Satellite gravity data[29] used to complement the ship data are available at http://topex.ucsd.edu/grav_outreach/#grid. The global relief dataset[38] ETOPO1 used to draw Figure 1 is available at https://www.ngdc.noaa.gov/mgg/global/global.html. The data that support the findings of this study are available from the corresponding author upon request.

## Code availability

The FORTRAN code used to calculate the gravity anomalies[30] is available from the corresponding author upon request.

413 References

414

415 28. Maia, M. COLMEIA cruise, RV L'Atalante, http://dx.doi.org/10.17600/13010010,
416 (2013).
417 29. Sandwell, D. T., Müller, R. D., Smith, W. H. F. , Garcia, E. & Francis, R. New global
418 marine gravity model from CryoSat-2 and Jason-1 reveals buried tectonic structure.
419 *Science* **346,** 65-67 (2014).
420 30. Maia, M. & Arkani-Hamed, J. The support mechanism of the young Foundation
421 Seamounts inferred from bathymetry and gravity. *Geophys. J. Int.* **149,** 190–210 (2002).
422 31. Parsons, B. & Sclater, J.G. An analysis of the variation of ocean floor bathymetry and
423 heat flow with age. *J. Geophys. Res.* **82,** 803–827 (1977).
424 32. Stein, C.A. & Stein, S. A model for the global variation in oceanic depth and heat flow
425 with lithospheric age. *Nature* **359,** 123–129 (1992).
426 33. Morgan, J.P. & Forsyth, D.W. Three-dimensional flow and temperature perturbations
427 due to a transform offset: Effects on oceanic crustal and upper mantle structure. *J.*
428 *Geophys. Res.* **93,** 2955–2966 (1988).
429 34. Ligi, M., Cuffaro, M., Chierici, F. & Calafato, A. Three-dimensional passive mantle flow
430 beneath mid-ocean ridges: An analytical approach. *Geophys. J. Int.* **175,** 783-805 (2008).
431 35. Mueller, R. D., Royer, J-Y., Cande, S.C., Roest, W.R. & Maschenkov, S. New constraints
432 on the late Cretaceous/Tertiary plate tectonic evolution of the Caribbean. In *Sedimentary*
433 *Basins of the World*, *Caribbean Basins* **4,** 33-59 (Elsevier, Amsterdam, 1999)
434 36. Gasperini L. *et al.* New data on the geology of the Romanche F.Z., equatorial Atlantic:
435 PRIMAR-96 cruise report, *Giornale di Geologia* **59,** 3-18 (1997).
436 37. Udintsev G.B. Equatorial Segment of the Mid-Atlantic Ridge. *IOC Technical Series* **46**
437 (UNESCO, New York, 1996).

438 38. Amante, C. & Eakins, B.W. ETOPO1 1 Arc-Minute Global Relief Model: Procedures,
439 Data Sources and Analysis. NOAA Technical Memorandum NESDIS NGDC-24. National
440 Geophysical Data Center, NOAA. doi:10.7289/V5C8276M (2009).
441
442

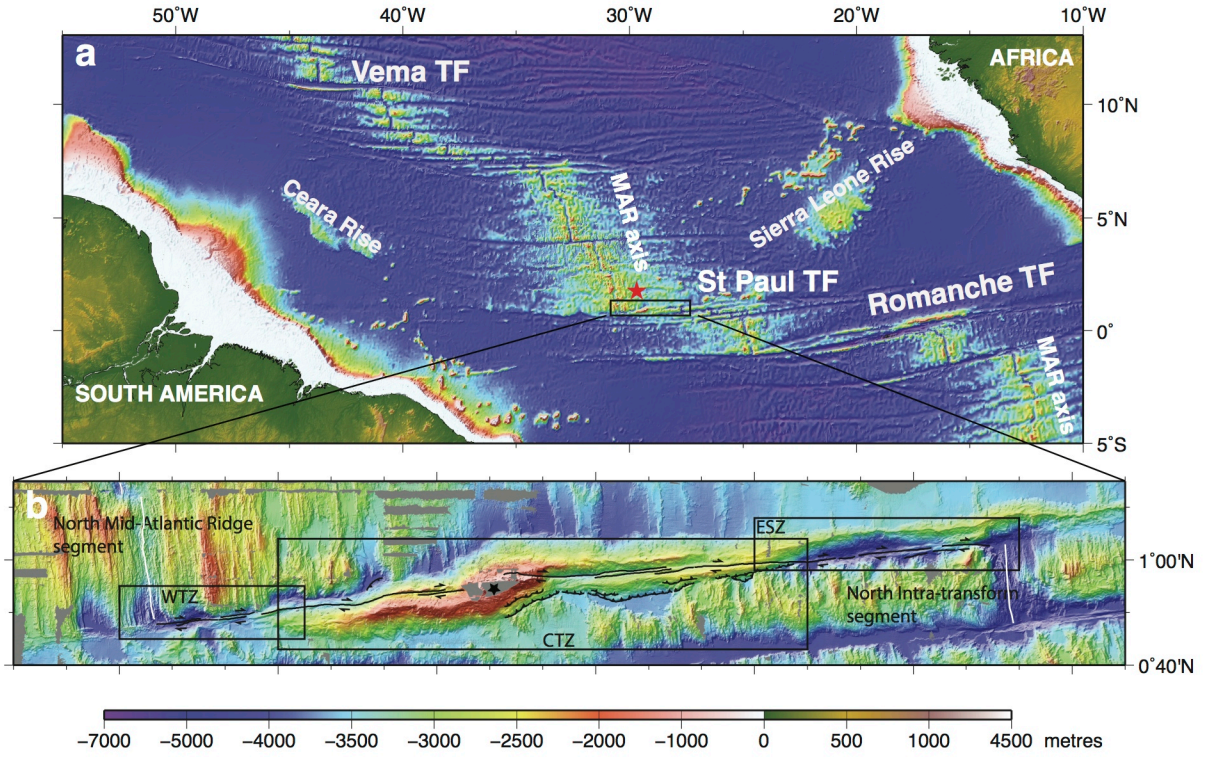
a
Vema TF
AFRICA
Ceara Rise
MAR axis
Sierra Leone Rise
St Paul TF
Romanche TF
SOUTH AMERICA
MAR axis
50˚W
40˚W
30˚W
20˚W
10˚W
10˚N
5˚N
0˚
5˚S
b
North Mid-Atlantic Ridge segment
ESZ
WTZ
North Intra-transform segment
CTZ
1˚00'N
0˚40'N
−7000
−5000
−4000
−3500
−3000
−2500
−2000
−1000
0
500
1000
4500
metres

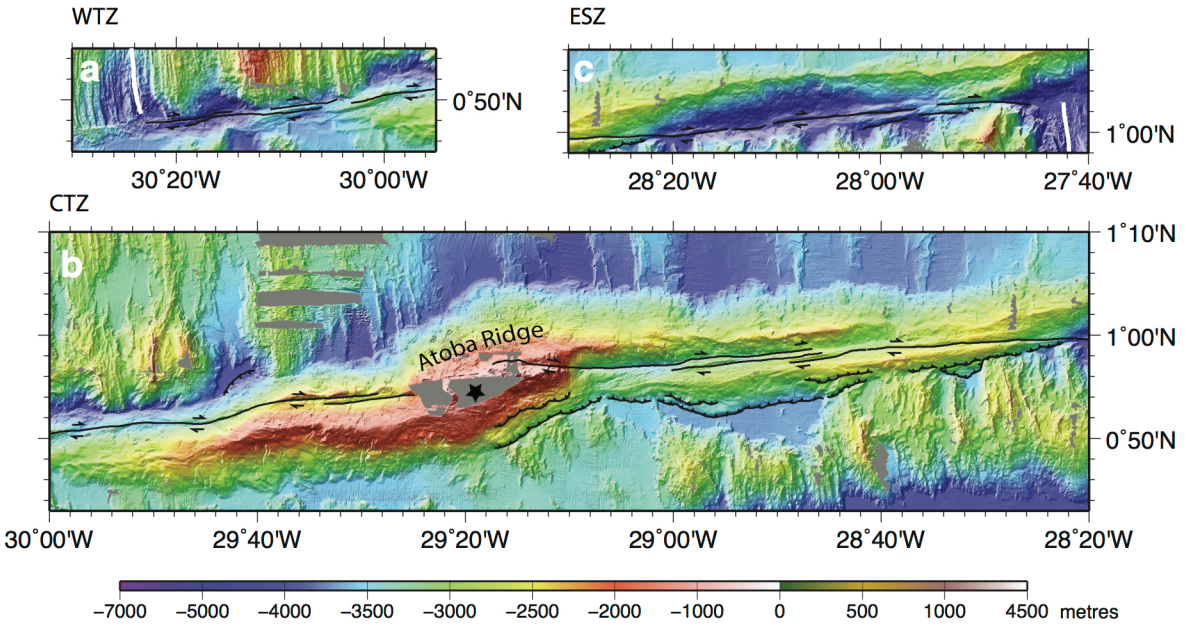
WTZ
a
0°50'N
30°20'W
30°00'W
ESZ
c
1°00'N
28°20'W
28°00'W
27°40'W
CTZ
b
1°10'N
1°00'N
0°50'N
Atoba Ridge
30°00'W
29°40'W
29°20'W
29°00'W
28°40'W
28°20'W
−7000
−5000
−4000
−3500
−3000
−2500
−2000
−1000
0
500
1000
4500
metres

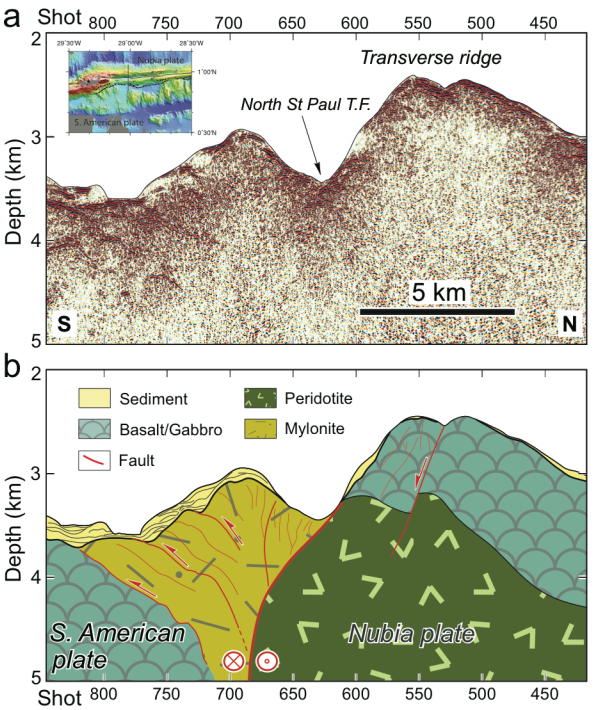
a
Shot
800
750
700
650
600
550
500
450
Depth (km)
2
3
4
5
Transverse ridge
North St Paul T.F.
5 km
S
N
Nubia plate
S. American plate
29°30'W
29°00'W
28°30'W
1°00'N
0°30'N


b
Depth (km)
2
3
4
5
Sediment
Basalt/Gabbro
Fault
Peridotite
Mylonite
S. American plate
Nubia plate
Shot
800
750
700
650
600
550
500
450

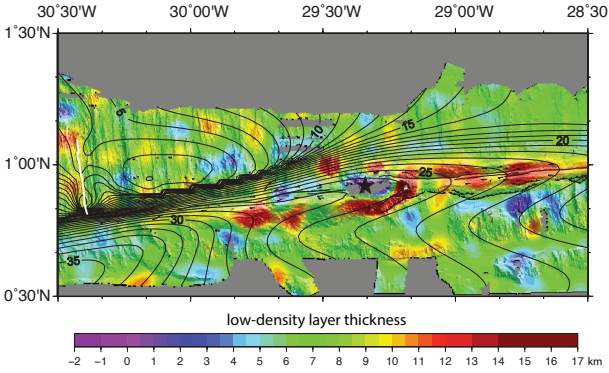
30°30'W
30°00'W
29°30'W
29°00'W
28°30'W
1°30'N
1°00'N
0°30'N
5
10
15
20
25
30
35
low-density layer thickness
–2 –1 0 1 2 3 4 5 6 7 8 9 10 11 12 13 14 15 16 17 km

prior to the 5° counterclockwise rotation
> 11 Ma

change in the spreading geometry
transtensive uplift of the flexural ridge
11-10 Ma

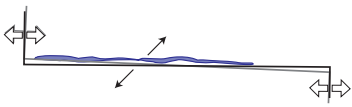

first southward propagation
compressional growth of the flexural ridge
10-8 Ma

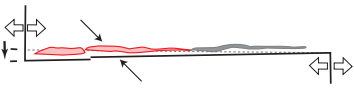

second propagation step
onset of the push-up ridge
8-5 Ma

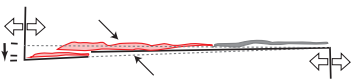

third propagation step
growth of the push-up ridge
formation of the graben
5-3 Ma

present day propagation
growth of the push-up ridge
en-echelon small pressure ridges